ENVIRONMENTAL RESEARCH
LETTERS

PURPOSE-LED PUBLISHING™
Celebrating the 20th anniversary of Environmental Research Letters

LETTER • **OPEN ACCESS**

Network cascading effects reveal thresholds and nonlinearity in ecological vulnerability

To cite this article: Xixi Liu *et al* 2026 *Environ. Res. Lett.* **21** 144004

View the article online for updates and enhancements.

You may also like

- An integrative methodology framework for assessing regional ecological risk by land degradation using the case of the Qinghai–Tibet Plateau
Yi Wang, Yihe Lü, Da Lü et al.
- Assessing the value and sensitivity of ecosystem services based on land use in the middle and lower reaches of the Shiyang River
Hu Tao, Guanglu Hu, Yalun Fan et al.
- Spatial flows of ecosystem services under future climate and land-use changes
Xiaodong Chen, Chenyang Zou and Yan Zhang

This content was downloaded from IP address 114.251.216.80 on 02/09/2026 at 05:09

ENVIRONMENTAL RESEARCH
LETTERS

Check for updates

OPEN ACCESS

RECEIVED
7 December 2025

REVISED
14 May 2026

ACCEPTED FOR PUBLICATION
29 June 2026

PUBLISHED
14 July 2026

Original content from this work may be used under the terms of the Creative Commons Attribution 4.0 licence.

Any further distribution of this work must maintain attribution to the author(s) and the title of the work, journal citation and DOI.

LETTER

Network cascading effects reveal thresholds and nonlinearity in ecological vulnerability

Xixi Liu[1,2,3], **Zheng Li**[1,2,3], **Yilin Zhao**[1,2,3], **David Makowski**[4], **Xingyu Ren**[1,2,3], **Mengyu Zhang**[5], **Hong Yang**[6] **and Wenfeng Liu**[1,2,3,*]

[1] State Key Laboratory of Efficient Utilization of Agricultural Water Resources, China Agricultural University, Beijing 100083, People's Republic of China
[2] National Field Observation and Research Station (Gansu Wuwei) for Efficient Water Utilization in Oasis Agriculture, Wuwei 733000, People's Republic of China
[3] Center for Agricultural Water Research in China, College of Water Resources and Intelligence Engineering, China Agricultural University, Beijing 100083, People's Republic of China
[4] UMR Applied Mathematics and computer Science Paris-Saclay (MIA-PS 518), INRAe AgroParisTech, Université Paris-Saclay, Palaiseau 91120, France
[5] Department of Ecology and Environment, PowerChina Huadong Engineering Corporation Limited, 311122 Hangzhou, Zhejiang, People's Republic of China
[6] 2w2e Environmental Consulting GmbH, Dübendorf, 8600 Zürich, Switzerland
* Author to whom any correspondence should be addressed.

E-mail: wenfeng.liu@cau.edu.cn

Keywords: land-use change, ecological vulnerability, cascading model, China, threshold

Supplementary material for this article is available online

Abstract

Anthropogenic land-use change is a primary driver of global ecosystem degradation. However, its systemic impact on ecological vulnerability across complex basin networks remains poorly quantified. A complex network framework was developed in this study to assess how land-use transitions influence ecological vulnerability in nine major river basins of China and the nation as a whole. A directed transition network of 26 land-use types for 2020–2023 was constructed and cascading failure simulations with changes in ecosystem service value change and ecological load entropy (ELE) were integrated together to quantify vulnerability. This approach reveals a nonlinear response of ecological vulnerability to land-use perturbations. Crop dryland, medium coverage grassland, and forest consistently emerge as critical hubs in both the land-use transition network and for vulnerability indicators, maintaining systemic stability. The results show that reallocating cropland generally increases ecosystem service value (ESV) at low disturbance levels before reaching a stability threshold, whereas disturbances to hydrological and forest land-use types cause the most severe losses. In arid regions, however, conversion of desert related land-use types initially increases ESV before declining after the threshold is exceeded. Analysis of recent changes (2020–2023) indicates that, on average, land-use transitions have improved ESV but have increased exposure to cascading failures in critical ecological nodes. A national stability threshold for medium coverage grassland at 0.5, alongside thresholds for other key land-use types across the basins were identified in this study. These findings provide a mechanistic and network perspective on land system vulnerability, offering scalable insights for designing spatially targeted conservation and strategies in China and other rapidly developing regions.

© 2026 The Author(s). Published by IOP Publishing Ltd

1. Introduction

Global ecosystem stability is increasingly at risk, with anthropogenic disturbances degrading nearly three quarters of the terrestrial surface (Winkler *et al* 2021, Niu *et al* 2024). At the global scale, the largest proportion of very high ecological and environmental vulnerability is concentrated in Asia (74.6%), followed by Africa (19.6%). At the country level, the highest levels of vulnerability are observed in China and India (Nguyen and Liou 2019). Land-use change is a dominant driver of this decline, reshaping biodiversity, ecological functioning, and ecosystem services (Sala *et al* 2000, Felipe-Lucia *et al* 2020, Li *et al* 2020, Yu *et al* 2022). Intensified human activities now permeate even remote catchments, generating cascading disturbances that erode ecological integrity and amplify vulnerability across river basins (Yang *et al* 2015, Cinner and Barnes 2019).

Ecological vulnerability refers to the degree to which ecosystems are prone to functional damage when exposed to external disturbances, reflecting their susceptibility and potential for loss rather than their capacity for recovery (Turner *et al* 2003). A range of theoretical frameworks has been developed to understand and assess ecosystem stability and vulnerability. Traditional approaches often rely on static aggregate framework indicators such as pressure-state-response (Hong *et al* 2016), exposure-sensitivity-adaptability (Zou and Yoshino 2017), or sensitivity-resilience-pressure (Song *et al* 2015) that summarize landscape condition at a given time. Ecosystem services were also applied to represents the ecological vulnerability in Guanzhong region of China (Wei *et al* 2024). However, ecosystem service values (ESV) primarily reflect the overall magnitude of ecological functions and therefore cannot adequately capture the heterogeneity and allocation of ecosystem services among different land-use types. To address this limitation, ecological load entropy (ELE) was introduced as an indicator that explicitly quantifies the diversity and distribution of ecosystem service contributions across land-use categories within Yellow River Basin of China (Niu *et al* 2024). By integrating ESV and ELE, it becomes possible to assess ecological vulnerability from both an aggregate perspective and a land-use specific structural perspective, thereby providing a more comprehensive evaluation of ecosystem vulnerability. Although many studies have mapped vulnerability patterns (Hong *et al* 2016, He *et al* 2018, Lv *et al* 2019, Zou *et al* 2021, Luo *et al* 2024), most treat ecosystems as static entities and overlook the dynamic pathways through which local perturbations spread across land-use systems. As a result, threshold responses, where ecosystem functioning declines sharply after disturbance exceeds a certain level, remain poorly understood. Such thresholds are central to ecological vulnerability theory, yet remain largely unexplored within land-use transition networks.

Complex network theory provides a powerful framework for capturing these cascading dynamics (Bodin *et al* 2019, Hamilton *et al* 2019, Felipe-Lucia *et al* 2022, Munguia-Vega *et al* 2022). By representing land-use types as nodes and transitions as weighted directed links, it becomes possible to quantify connectivity, identify critical risk nodes, and simulate transmission of disturbances. Previous work has applied this perspective to urban networks (Zhu *et al* 2023), forest and grass landscape (Yang *et al* 2022) and semi-arid rangelands (Cao *et al* 2022), but rarely at the watershed scale. Moreover, no study has jointly considered network topology, cascading failures, ESV and ELE to reveal threshold responses of land-use systems in nine major basins of China. ESV captures service supply, whereas ELE reflects the evenness of service load across land-use types (He *et al* 2025). The integration with network structure offers a multidimensional perspective on how disturbances accumulate and where thresholds emerge.

Rapid land-use transitions over recent decades in China have reshaped ecosystem service patterns, driving both gains in provisioning services in some regions and losses in regulating and supporting functions in others (Xie *et al* 2017). Urban expansion and cropland conversion have contributed to widespread habitat fragmentation and altered water cycles, increasing vulnerability in water scarce northern regions (Wu *et al* 2021) while reforestation efforts have enhanced carbon sequestration (Lu *et al* 2018) and vegetation cover in others. The large spatial extent and diverse ecosystems of China (Jiang *et al* 2021) thus make it a compelling case for detailed investigation of how land-use dynamics influence ecological vulnerability across complex landscapes. Such understanding is particularly critical in nine major river basins of China, where rapid land-use transitions driven by industrialization and demographic change have reshaped ecological processes (Ren *et al* 2002, Cheng *et al* 2021, Wang *et al* 2021, Yin *et al* 2022, Zhang *et al* 2023). Focusing on a single, large, and heterogeneous country allows the mechanisms linking network structure, cascading disturbances, and vulnerability thresholds to be examined in detail, providing insights that are broadly applicable to other rapidly transforming land systems.

To address these gaps, this study constructs directed and weighted land-use transition networks for 2020–2023 and applies a cascading-failure model (Zhao *et al* 2016) to simulate targeted perturbations. By quantifying shifts in ESV and ELE under increasing disturbance intensity, basin specific thresholds are

identified and mechanisms governing ecological vulnerability are diagnosed. The findings inform land-use strategies that balance socioeconomic development with long term ecosystem stability and offers actionable insights for sustainable land management in China and other large, complex landscapes.

2. Method

2.1. Study area and data sources

In this study, China and nine major river basins across the country were selected as the research area (figure 1). The nine major river basins include the Songhua and Liaohe River Basin, Haihe River Basin, Huaihe River Basin, Yellow River Basin, Yangtze River Basin, Pearl River Basin, Southeast Basin, Southwest Basin, and the Continental Basin. While the national land-use dataset covers the entire territory of China, including offshore island regions such as the Nansha Islands, the river basin framework is restricted to mainland river systems and therefore does not assign offshore islands to any basin. Covering approximately 9.6 million square kilometers, the landmass of China encompasses a wide range of ecosystems, including forests, grasslands, wetlands, deserts, agricultural lands, and urban areas (Lin and Ho 2003, Jiang *et al* 2021). The varied topography, ranging from high altitude plateaus and mountains to river valleys and coastal plains, contributes to its rich biodiversity and complex land-use patterns (Xu *et al* 2010).

Remote sensed land-use data of China at a spatial resolution of 1 km in 2020 and 2023 were obtained from Data Center for Resources and Environmental Sciences, Chinese Academy of Sciences (RESDC) (www.resdc.cn/). These datasets were classified into primary and secondary classes. At the primary class, land is classified into six categories based on land resources and the utilization properties which are cultivated land, forest land, grassland, water bodies, construction land, and unused land. The secondary class is primarily based on the natural attributes of land resources and is subdivided into 25 types. Net primary production (NPP) in 2020 and 2023 was obtained from MODIS of NASA (National Aeronautics and Space Administration, www.nasa.gov/) with a spatial resolution of 500 m. The NPP data were used to revise ecosystem service value equivalence factors.

The selection of the 2020–2023 period was motivated by the objective of identifying land-use thresholds under the current development pattern of land systems in China. This period represents the most recent nationwide land-use dataset with consistent classification standards and high spatial comparability across river basins. Thresholds inferred from earlier periods may no longer be applicable, as land-use transition pathways, dominant land-use types, and system constraints evolve over time in response to policy interventions, socioeconomic dynamics, and environmental regulation. Using the most recent transition matrix therefore ensures that the identified vulnerability thresholds are directly relevant to present day and near future land management.

2.2. Land-use transition networks

A land-use transition network was developed based on the land-use transfer matrix, comprising two main elements: nodes and edges. The nodes represent various land-use categories, while the edges indicate the transitions between these categories. Each edge is characterized by directionality and weight. The directionality signifies the shift from one land-use type to another, and the weight reflects the area transitioning between land-use types. In this study, we constructed the directed land-use transition network for 2020–2023 under Python platform considering the land-use changes between 2020 and 2023.

2.2.1. Network structural characteristics

Several key metrics were calculated to analyze the structure and dynamics of the land-use transition network. These metrics provided a comprehensive evaluation of the land-use transition network, helping to identify critical nodes and transitions within the system.

Node in-degree: number of transitions entering a land-use type, indicating how many other types transition into the targeted land-use type (Nie and Li 2023). A higher in-degree for a node suggests that multiple other nodes can directly transfer into it.

$$\mathrm{in}-\deg_m = \sum_{m\neq n\in N} l_{n\to m} \tag{1}$$

where, $\mathrm{in}-\deg_m$ refer to the weight of in-degree of node m. The variables m and n represent nodes m and n, respectively. $l_{n\to m}$ denotes the directed linkage from node n to node m, representing the presence of a transfer between the two nodes.

Node out-degree: number of transitions exiting from a land-use type, reflecting its contribution to transitions toward other land-use types.

$$\mathrm{out}-\deg_m = \sum_{m\neq n\in N} l_{m\to n} \tag{2}$$

where, $\mathrm{out}-\deg_m$ refer to the weight of out-degree of node m.

Average path length: average of the shortest path between any two nodes, providing insights into overall connectivity of the network (Pattanayak *et al* 2022). While direction and weight describe who transfers to whom and with what intensity, the

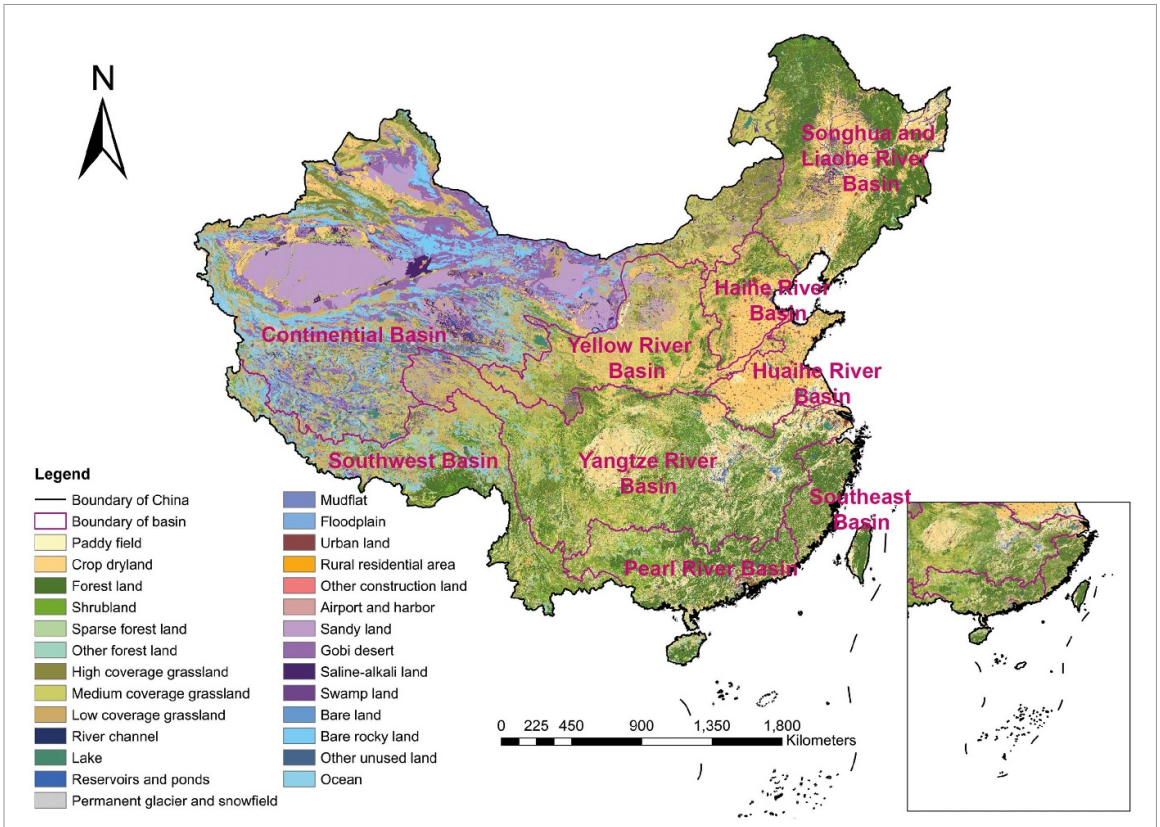

Figure 1. Spatial distribution of land-use types in 2023 and delineation of the nine major river basins across mainland China.

average path length reflects the overall structural accessibility of the land-use transition network, indicating how easily land-use types are connected through dominant transition pathways embedded in the weighted and directed network. The shortest path between two nodes were calculated considering the transition proportions as edge weights:

$$\mathrm{APL} = \frac{2}{N(N-1)} \sum_{m \neq n \in N} d_{mn} \tag{3}$$

in which, APL refers to the average path length; d_{mn} represents the shortest path between nodes m and n, which is 1/weight. N is the total number of nodes within the network, corresponding to the distinct land-use categories considered. This metric provides insights into the overall efficiency of the network, with a higher APL suggesting a more stable but less efficient network.

2.2.2. Identification of major land-use types

An integrated node centrality (INC) metric, which considers four standard centralities, was used to identify key land-use types of the network (Feng *et al* 2021). The four standard centralities metrics, including degree centrality (C_n^{deg}, which reflects the total number of transitions connected to a node and thus its direct activity level (Zhang *et al* 2011)), between centrality (C_n^{bet}, which measures the frequency with which a node lies on shortest paths, indicating its role as a conduit for transitions (Yang *et al* 2022)), eigenvector centrality (C_n^{eig}, which assigns higher scores to nodes connected to other influential nodes, capturing hierarchical influence (Estrada and Bodin 2008)) and pagerank (C_n^{pr}, which evaluates the probability of arriving at a node through random walks, representing its overall prominence in the directed network (Yang *et al* 2022)) for every node were calculated using NetworkX package of Python. A higher INC value signifies greater importance of the land-use type within the network.

$$\mathrm{INC}_n = C_n^{\mathrm{deg}} + C_n^{\mathrm{bet}} + C_n^{\mathrm{eig}} + C_n^{\mathrm{pr}} \tag{4}$$

where, INC_n represents the INC of node n.

2.3. Cascading failure model

The objective of this study is to assess ecological vulnerability, which is defined as the response of system to external disturbances that reduce the functional capacity or area stock of land-use components. From this perspective, vulnerability is evaluated through the consequences of losses or shocks, rather than through directional improvements of area of land-use. Therefore, disturbances are implemented as progressive reductions in the area stock of targeted land-use types, representing pressures arising

from human production activities, natural hazards, or extreme events.

This study applied the cascading failure model (Smart *et al* 2008) to examine the cascading effects within the land-use transition network under varying attack intensities to land-use areas of 2023 to analyze how an external shock to a specific land-use type would affect other transitions and ecosystem service values. In the model, disturbances were imposed by progressively decreasing the area stock of the targeted land-use type in 2023 by 10% at each attack step. Here, 10% represents low intensity disturbance to the land-use type, such as small scale environmental pollution, agricultural reclamation, or economic development leading to slow changes in ecological components; 50% represents moderate intensity disturbance, mainly caused by large scale natural disasters or human activities such as urban construction and industrial relocation guided by policies; 100% represents high intensity disturbance, usually resulting from the combined impact of extreme natural disasters and exceptionally large scale human activities, leading to the comprehensive collapse of system components and loss of functions. The reduced area was proportionally redistributed to other land-use types according to the original transition probabilities, which maintained the total land area and represented the spread of disturbances through connected land-use transitions.

In the network, node load represents the land-use areas. However, land-use areas are constrained by policies, regulations, and natural conditions, which define a maximum load capacity for each land-use type. When a disturbance causes a land-use type to exceed this capacity, the system equilibrium is disrupted, and the land-area load released by failed land-use types must be redistributed to other land-use types according to predefined transition rules. A tolerance parameter (α) was introduced to impose an upper bound on the area expansion of each land-use type; α (tested at 0.05, 0.08, 0.085, 0.09, 0.1, 0.2, and 0.3) defines the maximum permissible increase relative to the 2023 baseline.

2.4. Ecological vulnerability assessment

Following the cascading failure simulations described in section 2.3, this section quantifies how structural disruptions in the land-use transition network translate into functional ecosystem impacts. Within this framework, ESV captures the magnitude of ecosystem functions, while ELE reflects the balance and evenness of service contributions across land-use types. While section 2.3 examines how disturbances spread through the land-use network, ESV and ELE jointly assess the resulting magnitude of functional loss and redistribution imbalance. Together, these indicators provide a quantitative link between cascading structural failures and ecological vulnerability under land-use disturbances.

The ESV was calculated using the equivalent factor method (Xie *et al* 2015). In this framework, one equivalent factor (value = 1) is defined as the economic value of food production from one hectare of cropland, which serves as a standardized reference unit. Based on expert derived equivalence coefficients, ESV of 11 ecosystem service types was quantified including supply, regulating, supporting and cultural services for each land-use type using the 2015 equivalent factor table (table S1). To align the land-use reclassification system used in this study with the ecosystem categories in the equivalent factor table, high, medium, and low coverage grasslands was categorized as grasslands, shrub grasslands, and meadows, respectively, according to the equivalent factor table (Xiong *et al* 2024). Similarly, forested land was treated as the average of coniferous forests, mixed coniferous and broad leaved forests, and broad leaved ecosystems. Based on this reclassification, the equivalent ESV per unit area of terrestrial China in this study was determined (Xiong *et al* 2024).

The baseline economic coefficient Ga was derived from the combined average economic output of rice, wheat, and maize, which was 17 500.95 Yuan/ha in 2020 and 20 400.90 Yuan/ha in 2023 (National Development and Reform Commission 2024). Following the standard definition, Ga equals one seventh of the average grain yield value (Xie *et al* 2003, Xiong *et al* 2024) resulting in 2,500.14 Yuan/ha for 2020 and 2914.41 Yuan/ha for 2023. This coefficient provides a uniform monetary benchmark for converting equivalence factors into comparable ESV estimates across years. Spatial NPP data were incorporated to refine the equivalence factors. For each year, NPP grids were normalized to represent relative productivity, and the normalized values were applied as annual adjustment coefficients. This allows regions with higher productivity to receive proportionally larger ESV values, improving the ecological realism of the valuation.

All ecosystem service values are expressed in Chinese Yuan (CNY). For international comparison, values can be converted to US dollars using the average exchange rate of 1 CNY = 0.1415 USD in 2023 (www.exchangerates.org.uk/). To evaluate the ecological vulnerability of the land-use system, changes in ecosystem service values due to the attack ESV change (ESVC) were calculated.

$$\text{Attack_ESVC}_{2023\rightarrow\text{attack}} = \text{ESV}_{\text{attack}-2023} - \text{ESV}_{2023} \tag{5}$$

in which, $\text{Attack_ESVC}_{2023\rightarrow\text{attack}}$ represents changes in ESV, $\text{ESV}_{\text{attack}-2023}$ and ESV_{2023} refer to the ESV of 2023 after applying the attack scenario and ESV of 2023, respectively.

While ESVC provides an effective measure of the overall ecological capacity of the land ecosystem,

it does not account for the variations in ecological services across different land-use types within the system. To further evaluate the effects of land-use changes on ecological vulnerability at both the overall system and individual level, ELE was also included in this study (Niu *et al* 2024). ELE represents the heterogeneity of service load distribution across land-use types (Bao *et al* 2008). When this distribution becomes highly uneven, the system is more likely to experience cascading failures because effects of shocks concentrate on a few overloaded nodes. Recent work further suggests that land-use transition networks with elevated ELE values are less susceptible to external disturbances, as greater heterogeneity reduces the ability of this system to redistribute load efficiently (Novi Inverardi and Tagliani 2023, He *et al* 2025).

$$\mathrm{ELE} = -\sum_{i=1}^{26}[P_i \ln(P_i)] \tag{6}$$

$$P_i = \frac{\mathrm{ESV}_i}{\sum_{i=1}^{26}\mathrm{ESV}_i} \tag{7}$$

where P_i represents the proportion of ecosystem services provided by land-use type i relative to the total services. Together, ESVC and ELE allow for a more comprehensive assessment of ecological vulnerability.

3. Results

3.1. Land-use changes between 2020 and 2023

Network analysis identified crop dryland as the land-use category with the highest degree (both in and out) in most basins, functioning as a net 'source' of transitions (table 1). The exceptions were the Southeast, Southwest, and Continental basins, where the highest output degree roles were occupied by forest land, medium coverage grassland and low coverage grassland, respectively. At the national level, the primary transitions from crop dryland were to rural residential areas (16.2%), medium coverage grassland (14.5%), and paddy fields (12.8%) (table S2). Conversely, the primary sources of new crop dryland were rural residential areas (16.9%), medium coverage grassland (14.4%), and forest land (12.9%) (table S2).

The out/in degree ratio, which ranged from 0 to 2.6, further illuminated these dynamics. Notably, the land-use types with the highest ratios in each basin were often those with low absolute degree values. In four basins, water body related categories exhibited the highest ratios. In contrast, human dominated land-use types, which are specifically reservoirs and ponds, urban land, and other construction land, consistently showed a higher in-degree than out-degree, confirming their role as dominant structural sinks in the land-use system at both national and basin scales.

3.2. Complex land-use networks and key land-use types

APL values at the basin scale for 2020–2023 showed a clear gradient from western to eastern basins in the compactness of land-use transition networks (figure 2). The Continental and Yangtze River basins exhibit the highest APL (2.31–2.85), signifying more dispersed transitions. In contrast, the Pearl River and Southeast basins in southern coastal China showed the lowest APL values (1.06–1.14), indicating stronger connectivity. The INC values, which identify critical land-use types within the network, range from 0.006 to 2.681. At the national scale, the five land-use types with the highest INC are crop dryland, medium coverage grassland, shrubland, paddy field, and forestland. This pattern holds broadly across basins, where crop dryland, various grassland classes (medium/low coverage), and forest land consistently emerge as the most central nodes. Clear regional differences were observed for land use types strongly affected by human activities: urban land and other construction land ranked among the five most central nodes mainly in the coastal Southeast and Huaihe basins, reflecting stronger human influence on land use transitions in these regions. This is further underscored by a clear gradient from inland to coastal regions in the mean INC across all land-use types, with values declining from west to east.

Overall, crop dryland, forest land, grassland consistently exhibited elevated INC, indicating high structural centrality within the land-use transition network. The numerous transition connections with other land-use types suggest that these classes function as key hubs that mediate land-use conversions and maintain overall network connectivity. Owing to their central positions and extensive linkages, changes in these land use types are likely to spread through the network, influencing multiple transition pathways and amplifying responses across the entire system. Consequently, perturbations affecting these structurally critical land-use types are expected to generate disproportionately large cascading effects compared to less connected categories.

3.3. Ecological vulnerability under different disturbance levels

3.3.1. Ecosystem service value

From 2020 to 2023, China experienced a net increase in ESV across all major basins (figure 3). The ESVC ranged from a loss of 1.13×10^8 Yuan/(grid cell) to a gain of 1.35×10^8 Yuan/(grid cell), resulting in an average national net increase of 6.64×10^5 Yuan/(grid cell). Spatially, the southern coastal basins showed the most robust growth, with the Pearl and Southeast River basins recording the highest mean gains (1.47×10^6 and 1.51×10^6 Yuan/(grid cell), respectively). In contrast, the Continental Basin registered the smallest mean change (4.26×10^4

Table 1. Land-use transition network metrics for China and its major basins. The figure shows the in-degree, out-degree, and out-degree/in-degree ratio of all land-use types based on the 2020–2023 land-use transition data. Each row corresponds to a single land-use type, with major classes indicated by the colored swatches on the left. For each basin, the three adjacent columns represent the out-degree, in-degree, and output/input ratio.

		China			Songhua and Liaohe River Basin			Haihe River Basin			Huaihe River Basin			Yellow River Basin		
Landuse	Landuse	Input	Output	Output/input	Input	Output	Output/input	Input	Output	Output/input	Input	Output	Output/input	Input	Output	Output/input
Cropland	Paddy field	35 576	33 762	0.95	6319	5375	0.85	145	149	1.03	3577	3614	1.01	488	501	1.03
	Crop dryland	111 150	113 573	1.02	22 151	22 281	1.01	10 560	10 689	1.01	10 675	10 916	1.02	21 698	21 937	1.01
Forestland	Forest land	54 284	59 427	1.09	14 021	19 022	1.36	2803	3055	1.09	1444	1424	0.99	3310	3298	1.00
	Shrubland	48 778	48 644	1.00	4684	4558	0.97	3057	2928	0.96	785	769	0.98	6896	7018	1.02
	Sparse forest land	33 581	30 285	0.90	5547	2081	0.38	1082	1037	0.96	518	517	1.00	3140	3103	0.99
	Other forest land	4422	4433	1.00	885	758	0.86	271	302	1.12	168	196	1.17	691	692	1.00
Grassland	High coverage grassland	51 516	51 901	1.01	4851	5220	1.08	3823	3845	1.01	919	966	1.05	7781	7712	0.99
	Medium coverage grassland	77 784	75 973	0.98	4308	2452	0.57	2326	2290	0.98	838	807	0.96	19 208	19 052	0.99
	Low coverage grassland	60 895	60 979	1.00	453	241	0.53	1489	1475	0.99	306	317	1.04	14 311	14 468	1.01
Water bodies	River channel	6505	6833	1.05	799	1108	1.39	588	572	0.97	633	610	0.96	631	692	1.10
	Lake	3012	2992	0.99	710	472	0.66	25	20	0.80	128	129	1.01	115	101	0.88
	Reservoirs and ponds	5124	4740	0.93	875	618	0.71	450	435	0.97	1072	983	0.92	373	372	1.00
	Permanent glacier and snowfield	3417	3395	0.99	0	0	—	0	0	—	0	0	—	9	11	1.19
	Mudflat	165	320	1.95	19	14	0.73	1	2	1.75	21	32	1.51	2	4	2.60
	Floodplain	8238	7558	0.92	1134	856	0.76	489	317	0.65	410	443	1.08	720	671	0.93
Built-up land	Urban land	4142	3835	0.93	427	890	2.08	561	512	0.91	962	885	0.92	488	420	0.86
	Rural residential area	27 556	28 090	1.02	4937	5540	1.12	4665	4733	1.01	8694	8652	1.00	3616	3574	0.99
	Other construction land	6808	5322	0.78	432	656	1.52	1142	1093	0.96	703	599	0.85	1103	808	0.73
Unused land	Sandy land	8277	8578	1.04	73	87	1.19	5	6	1.13	2	2	0.71	1056	1125	1.07
	Gobi desert	16 475	16 904	1.03	0	0	—	0	0	—	0	0	—	188	220	1.17
	Saline-alkali land	6445	6692	1.04	1518	1810	1.19	15	19	1.24	3	2	0.87	59	71	1.20
	Swamp land	8469	8237	0.97	3839	3945	1.03	122	131	1.08	9	8	0.86	916	914	1.00
	Bare land	6385	6406	1.00	32	37	1.13	11	10	0.91	11	11	1.00	369	370	1.00
	Bare rocky land	29 725	29 929	1.01	49	39	0.79	7	17	2.36	34	36	1.06	714	743	1.04
	Other unused land	2546	2574	1.01	0	0	—	0	0	—	0	1	—	109	114	1.05
Ocean	Ocean	138	28	0.20	0	0	—	0	0	—	6	0	0.00	1	0	0.00

(Continued.)

Table 1. (Continued.)

Landuse	Landuse	Yangtze River Basin			Pearl River Basin			Southeast Basin			Southwest Basin			Continental Basin		
		Input	Output	Output/input	Input	Output	Output/input	Input	Output	Output/input	Input	Output	Output/input	Input	Output	Output/input
Cropland	Paddy field	17 183	17 207	1.00	6761	5764	0.85	170	227	1.34	885	869	0.98	17	21	1.22
	Crop dryland	28 396	28 828	1.02	6737	8212	1.22	33	42	1.28	4681	4636	0.99	6127	5977	0.98
Forestland	Forest land	18 064	18 200	1.01	5561	5436	0.98	267	278	1.04	6021	5965	0.99	2756	2729	0.99
	Shrubland	18 727	18 812	1.00	5130	5079	0.99	130	126	0.97	6650	6656	1.00	2698	2683	0.99
	Sparse forest land	12 174	12 311	1.01	4771	4793	1.00	15	27	1.84	4789	4858	1.01	1536	1551	1.01
	Other forest land	761	781	1.03	792	824	1.04	13	23	1.77	518	527	1.02	318	321	1.01
Grassland	High coverage grassland	12 412	12 241	0.99	3422	3487	1.02	60	60	1.01	7528	7569	1.01	10 645	10 722	1.01
	Medium coverage grassland	23 133	23 252	1.01	2343	2353	1.00	4	5	1.25	9090	9057	1.00	16 508	16 689	1.01
	Low coverage grassland	8405	8322	0.99	335	307	0.92	2	3	1.50	8814	8853	1.00	26 751	26 959	1.01
Water bodies	River channel	1301	1309	1.01	377	359	0.95	9	7	0.77	815	781	0.96	1289	1242	0.96
	Lake	418	626	1.50	17	20	1.15	0	1	2.00	221	226	1.02	1375	1396	1.02
	Reservoirs and ponds	1141	1154	1.01	475	436	0.92	7	9	1.33	135	125	0.93	395	416	1.05
	Permanent glacier and snowfield	137	150	1.10	0	0	—	0	0	—	924	887	0.96	2336	2333	1.00
	Mudflat	2	2	1.20	9	11	1.21	0	2	—	0	0	—	0	0	—
	Floodplain	1405	1278	0.91	49	61	1.24	8	4	0.44	485	478	0.99	3497	3425	0.98
Built-up land	Urban land	1001	818	0.82	408	89	0.22	13	11	0.85	51	50	0.98	194	148	0.76
	Rural residential area	3437	3425	1.00	927	934	1.01	37	23	0.61	148	144	0.98	1071	1047	0.98
	Other construction land	1572	1064	0.68	477	431	0.90	87	8	0.09	129	108	0.83	1002	418	0.42
Unused land	Sandy land	462	470	1.02	1	1	1.33	0	0	—	66	69	1.05	6609	6815	1.03
	Gobi desert	1010	1008	1.00	0	0	—	0	0	—	564	573	1.02	14 709	15 101	1.03
	Saline-alkali land	107	102	0.95	2	1	0.40	0	0	—	112	115	1.02	4626	4570	0.99
	Swamp land	723	628	0.87	1	2	1.75	0	0	—	595	591	0.99	2221	1976	0.89
	Bare land	53	52	0.99	4	4	0.92	0	0	—	1021	1001	0.98	4883	4920	1.01
	Bare rocky land	2274	2232	0.98	11	11	0.97	0	0	—	6138	6237	1.02	20 467	20 579	1.01
	Other unused land	348	372	1.07	0	0	—	0	0	—	48	52	1.09	2040	2034	1.00
Ocean	Ocean	0	0	—	8	2	0.24	0	0	—	0	0	—	0	0	—

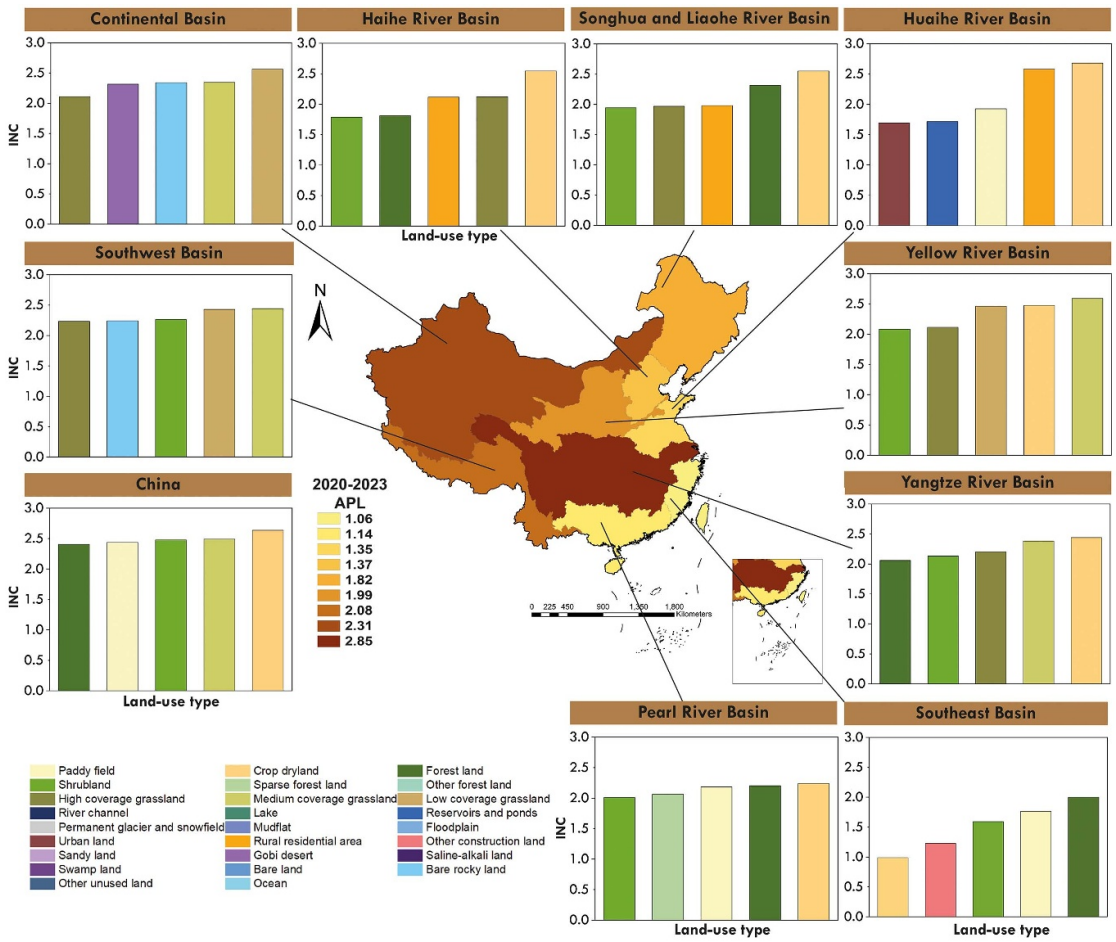

Figure 2. Network centrality and connectivity across major basins in China. The central map displays the spatial distribution of the average path length (APL) for the period 2020–2023, illustrating regional differences in network connectivity. The surrounding panels detail the top five land-use types, ranked by their integrated node centrality (INC) within each corresponding basin.

Yuan/(grid cell)), while the Southwest Basin displayed the greatest volatility, experiencing both the most severe localized loss and the highest local gain. These patterns underscore a pronounced spatial heterogeneity, with southern basins tending toward net improvement and western/northern basins exhibiting greater variability and isolated declines.

Figure 3 also synthesizes the response of ESV to simulated perturbations of specific land-use classes. The sensitivity in ESV was basin specific to these perturbations. The Haihe and Yellow River Basins exhibited relatively gentle response slopes, suggesting a higher tolerance to moderate shocks. Conversely, the Yangtze and Pearl River Basins displayed steeper slopes, signaling higher sensitivity. Nonlinear behavior was evident in several basins, where small disturbances initially increased ESV through redistribution, but larger shocks reversed the gains once systemic capacity limits were approached.

We identified critical perturbation thresholds for key land-use types, beyond which ESVC trends change fundamentally (figure 3, table 2). For instance, the threshold for crop dryland was 0.3 in the Haihe River Basin and 0.6 in the Songhua and Liaohe River Basin when the α is 0.15. Crucially, the relationship between perturbation intensity and ESV is not always linear. A key finding is the nonmonotonic response in the Southwest Basin when targeting shrubland (table 2 (b)). While higher intensity attacks cause degradation, a precise combination of load capacity and attack power can yield a positive ESVC. This pattern results from cascading redistribution processes in which shrubland is transferred to land-use types with higher ecosystem service values, such as forest land, following the observed transition relationships within the basin. Therefore, the highest attack power threshold identified is not merely a failure point but a critical leverage point for strategic management, beyond which the buffering capacity of this system is exhausted and services collapse.

3.3.2. ELE

At baseline (attack intensity = 0), ELE varies significantly across river basins in China, ranging from 1.474 to 2.252, with the national aggregate recording the highest value of 2.425 (figure 4). Spatially, a clear pattern emerges: coastal basins in the south and southeast (Southeast Basin: 1.474; Pearl River

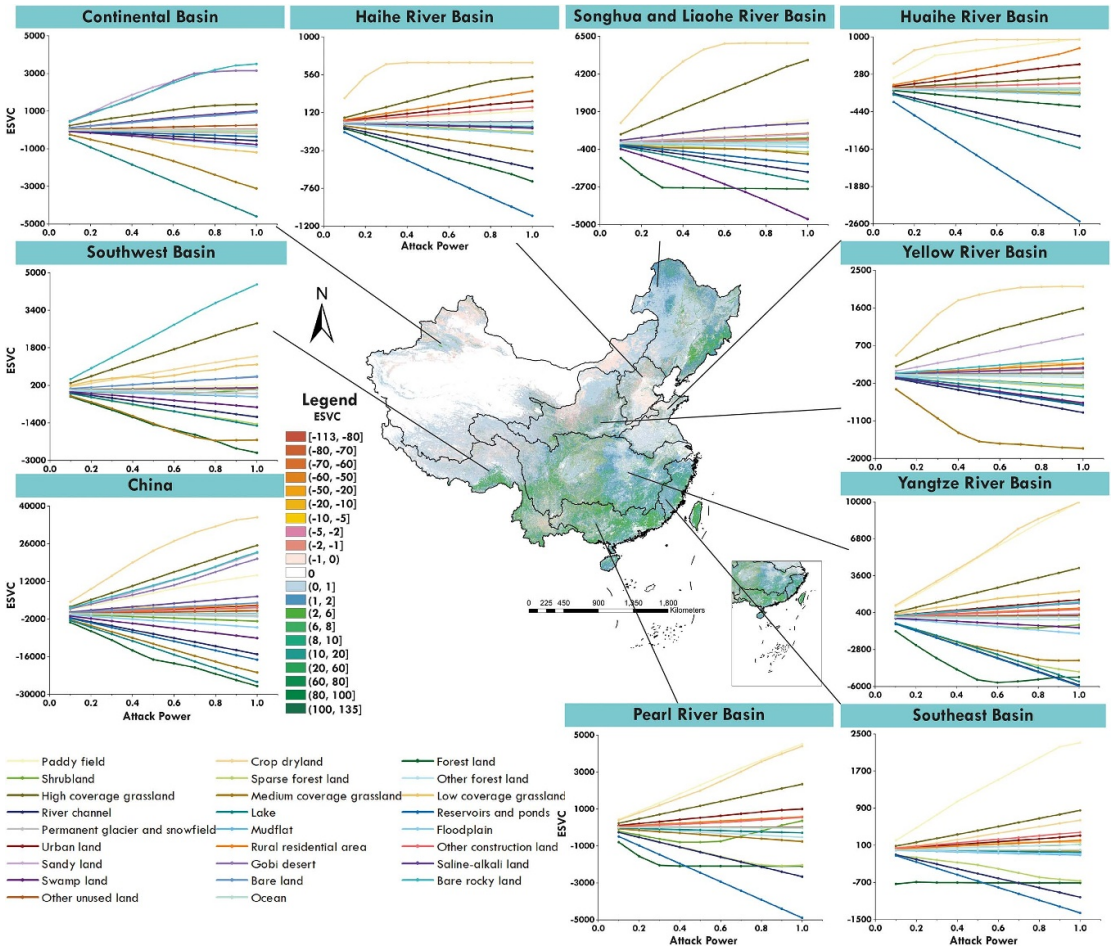

Figure 3. Simulated ESV sensitivity to land-use node perturbations. The central map shows the spatial distribution of the net ESVC, calculated as the difference between 2023 and 2020 values (units: 10^6 Yuan). The surrounding panels illustrate the cascading impact simulations for each major river basin. For each simulation, the 2023 land-use composition and the 2020–2023 transition probability matrix were used, with a system capacity parameter (α) of 0.15. In these plots, the *x* axis represents the disturbance intensity (attack power, unitless) applied to a specific land-use node, ranging from 0.1 to 1.0. The *y* axis shows the resulting change in total ESV (ESVC, units: 10^8 Yuan), calculated as the difference between the perturbed ESV and the 2023 baseline. Each line corresponds to the simulated perturbation of a single land-use type, with colors and styles consistent across all panels as defined in the legend.

Table 2. Critical thresholds triggering shifts in ecosystem service value change (ESVC) response. The table identifies the specific combinations of land-use load capacity (α) and attack power at which the ESVC response to perturbations fundamentally changes direction. (a) Conditions under which a unidirectional reversal of ESVC occurs. When the ESVC change direction is positive to negative, it represents the ESVC would change from positive to negative when the corresponding attack power reached and vice versa. (b) Conditions under which ESVC becomes transiently positive within a specific parameter range, contrasting with negative values under other settings. When the ESV increased after attack, the ESVC attribute is positive and vice versa. The bold values indicate the threshold attack power values beyond which the ESVC response shifts from positive to negative.

a	River name	Landuse	α	Attack power	ESVC change direction
	Haihe River Basin	Low coverage grassland	0.05	**0.8**	Positive to negative
	Yangtze River Basin	Shrubland	[0.05,0.1]	[0.5,1]	Negative to positive
	Yangtze River Basin	Permanent glacier and snowfield	0.05	0.7	Negative to positive
	Pearl River Basin	Mudflat	[0.05,0.085]	[**0.6,1**]	Positive to negative
	Pearl River Basin	Shrubland	[0.08,0.1]	[0.5,0.6]	Negative to positive
	Southeast Basin	Other forest land	[0.08,0.085]	**1**	Positive to negative
	Continental Basin	Low coverage grassland	[0.08,0.3]	[**0.2,0.4**]	Positive to negative
b	River name	Landuse	α	Attack power	ESVC attribute
	Southwest Basin	Shrubland	0.05	**0.4**	Positive
	Southwest Basin	Shrubland	0.08	[0.6,**0.7**]	Positive
	Southwest Basin	Shrubland	0.085	[0.6,**0.7**]	Positive
	Southwest Basin	Shrubland	0.09	[0.6,**0.8**]	Positive
	Southwest Basin	Shrubland	0.1	[0.7,**0.8**]	Positive

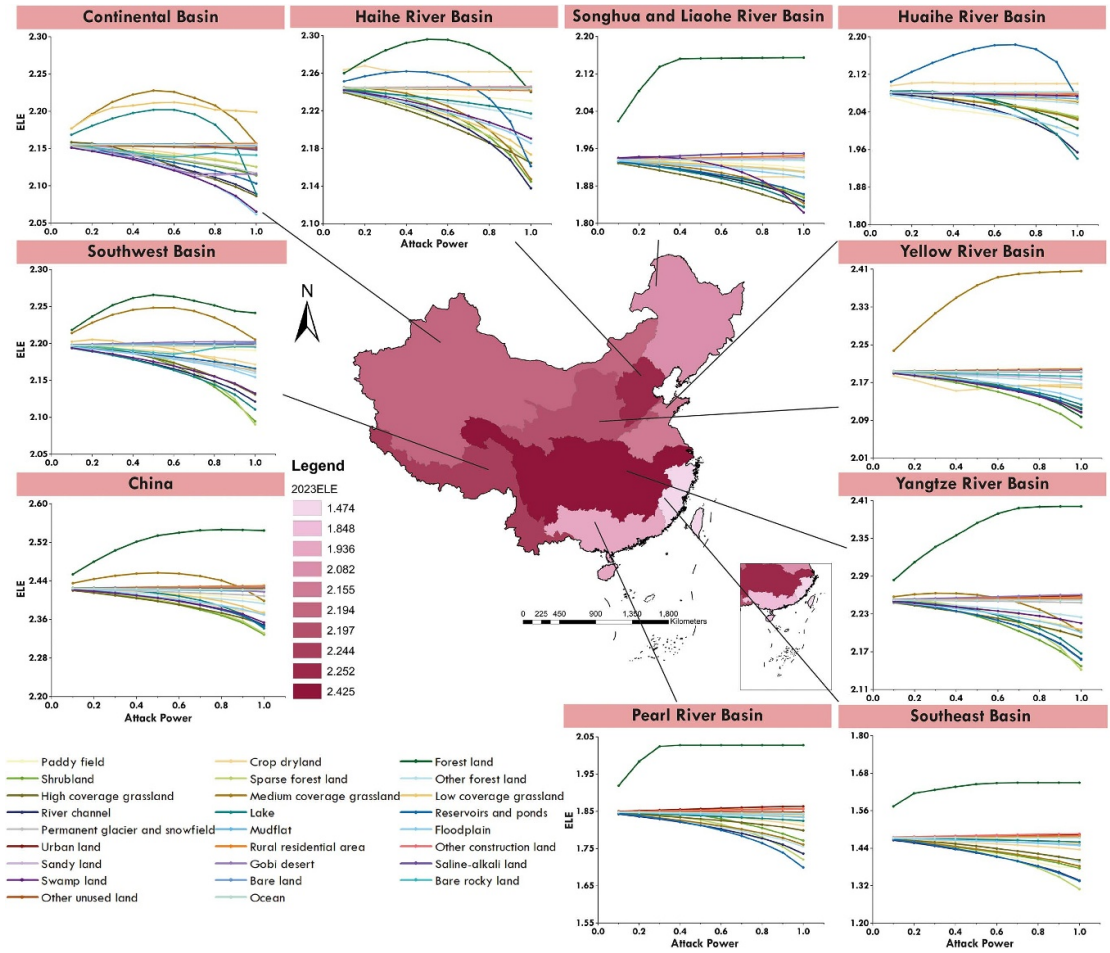

Figure 4. Sensitivity of ELE to land-use node perturbations. The central map illustrates the baseline spatial distribution of ELE across the nine major river basins for the year 2023. The surrounding panels present simulation results of the cascading impacts on ELE for each basin. Simulations are based on the 2023 land-use composition and the land-use transition probability matrix derived from observed changes between 2020 and 2023, with a system capacity parameter (α) of 0.15. In these plots, the x axis represents the disturbance intensity (attack fraction, unitless), ranging from 0.1 to 1.0. The y axis shows the resulting value after the perturbation is applied. Each line corresponds to the simulated perturbation of a single land-use type, with colors and styles consistent across all panels as defined in the legend.

Basin: 1.848) exhibit the lowest ELE, indicating a more concentrated ecosystem service portfolio. In contrast, the large northern and central river systems (e.g. Yangtze River Basin: 2.252; Haihe River Basin: 2.244) show higher ELE, reflecting a more even distribution of service contributions across land-use categories. The high national value results from the aggregation of these heterogeneous regions, which increases the overall evenness at the country scale.

Changes in ELE (figure 4) show that the sensitivity of it is strongly basin dependent and land-use specific, with coastal basins tending to lose evenness rapidly under perturbation while several inland basins show limited increases at low intensities followed by decline once capacity limits are approached. Although responses vary across regions and land-use categories, three robust patterns emerge. First, in most basins ELE declines monotonically for the majority of land-use types, implying that progressive perturbations concentrate ecosystem service contributions in fewer categories and reduce the evenness of the portfolio. Second, several northern and central basins, notably the Haihe and Continental exhibit nonlinear responses for a subset of categories: ELE rises at low perturbation levels and then decreases beyond intermediate intensities, revealing threshold behavior in the cascading network. Third, large basin systems such as the Yangtze and the Continental Basin display relatively gentle slopes for many categories, suggesting greater tolerance of moderate shocks before evenness deteriorates.

It is obvious that the ELE would increase when attack medium coverage grassland at the national scale and this land-use type function as critical risk node within the attacked network (figure 4). Modest reductions in medium coverage grassland (<50%) led to increasing ELE, suggesting temporary gains in

balance through redistribution. Yet once contraction exceeded around 50%, ELE declined, revealing a tipping point beyond which ecosystem functioning deteriorated and network stability collapsed when the α is 0.15. This reflects the dominant area and irreplaceable service contribution of medium coverage grassland in China. Moreover, the higher α value corresponds to a higher threshold of land-use nodes.

4. Discussion and conclusion

4.1. Linking network structure to ecological vulnerability

Our land-use ecological complex network framework integrates observed 2020–2023 transitions with ecosystem service valuation and cascading failure simulations. This dual approach reveals that recent land reallocations and network encoded transition pathways jointly shape ecological vulnerability. Nationally, ESV increased with gains concentrated in regions of forest and grassland expansion, while water related ecosystems remained critical service providers because of the high value of hydrological regulation service.

Network analysis delineates a clear inland and coastal contrast. Inland basins feature longer average path lengths and more diversified service portfolios (higher ELE), whereas coastal basins exhibit compact networks and lower ELE, implying higher sensitivity to disturbance. Simulations confirm this structural vulnerability: disturbing hydrological or high coverage vegetation nodes produces the most severe ESV losses, while perturbing cropland often enhances ESV by reallocating land toward forest and grassland. Although our results show that ESV increased from 2020 to 2023, previous studies have reported that only 1.32% of population of China lived in areas with low ecological vulnerability during 2012–2014 and also indicated that the central and northwestern regions are more vulnerable to losses of ecosystem services than other parts of China (He *et al* 2018). Land-use change from desert to grassland pathways in arid basins yield marked ecological gains, illustrating regional specific restoration opportunities. Particularly in the Continental Basin, the NPP value which is related to the habitat quality of this basin is minimum of nine basins in China and unused land whose equivalent factor is relatively low mainly located in this basin, therefore, the average of ESV of this basin per km^2 is minimum. In this basin, grassland and unused land with higher INC, and attack these nodes would increase the ESVC and ELE. The priority areas for ecological restoration have been identified (Han *et al* 2026), as supplementary, threshold of related land-use to increase the habitat quality and land-use diversity has been identified in this study.

Crucially, land-use types with higher INC, such as crop dryland, medium coverage grassland, and forest land, consistently correspond to greater systemic vulnerability when attacked, demonstrating a tight coupling between network structure and ecological fragility (Peng *et al* 2024, He *et al* 2025). This finding provides a potential explanation for the persistence of vulnerability and socioeconomic stress in regions with high production potential and intensive land use, such as the Southeast Basin and the Songhua and Liaohe River Basin. As highlighted by recent human and nature coupling studies (Sietz *et al* 2025), high biophysical productivity does not necessarily translate into system level stability or social wellbeing when land-use systems are structurally concentrated and lack redundancy. In such contexts, shocks to central land-use types whether driven by climate extremes, policy shifts, or market pressures, can rapidly undermine both ecological functions and livelihood security.

4.2. Mechanistic drivers of nonlinear responses

A key finding is that relative lower intensity perturbations to dominant land-use types which are defined either by large area shares or by high total ecosystem service value contributions, can initially increase ELE. This occurs because a moderate reduction in dominant land-use area leads to a more even redistribution of land among other land-use types through the observed 2020–2023 transition network. At this stage, the receiving land-use types remain below their capacity constraints defined by the tolerance parameter (α), allowing the system structure and ecosystem service contributions to become temporarily more balanced. This redistribution temporarily spreads ecosystem service contributions more evenly across land-use categories, resulting in an initial increase in ELE. However, as perturbation intensifies and receiving nodes saturate, ELE declines, revealing a systemic tipping point. This cascading behavior is consistent with other networked systems (Zhao *et al* 2005, Wang and Rong 2009). The practical implication is that the general ESV benefit of reallocating cropland is conditional: gains occur only when transition pathways channel area toward higher value classes and when system capacity allows for absorption without triggering large overflows.

Furthermore, ESVC and ELE provide complementary insights. For instance, perturbations to shrubland in the Yangtze and Pearl River basins can show positive ESVC due to transitions to higher value categories, yet ELE plateaus or declines (table 2 (a) and figure 4), indicating functional enhancement without structural reinforcement (Malik *et al* 2017, Shang 2019, Jarillo *et al* 2022). This divergence underscores the necessity of joint evaluation for accurately capturing changes in ecological vulnerability under land-use disturbances (Fu *et al* 2024).

4.3. Policy implications for basin specific governance

It has been revealed that ecological vulnerability in China is driven by population pressure, resource depletion, extensive economic growth, environmental pollution, insufficient environmental protection investment, and accelerated population aging (He *et al* 2018). These pressures are also related with land-use transition. Our findings support basin specific land-use strategies that integrate national principles with local network topology. Conservation of water and wetland nodes must serve as a strict national constraint. In coastal basins with low ELE (e.g. Pearl, Southeast), strict protection of water related land and compact urban expansion are crucial to mitigate rapid entropy decline. In forest dominated basins (e.g. Haihe, Yangtze), management should maintain forest cover while avoiding single class dominance through close to nature practices (He *et al* 2025). In grassland influenced basins (e.g. Yellow River, Continental), management should prioritize grassland stability through regulated grazing and targeted restoration (Hou *et al* 2021). Adjusting land-use tolerance which is represented by α, through zoning and ecological red lines can directly manage systemic capacity and prevent harmful cascades. This network informed approach provides a scalable framework for spatially targeted ecosystem management and land-use policy.

4.4. Limitations and future directions

Based on observed land-use transitions (2020–2023) across China and its nine major river basins, a land-use transition complex network was developed with ecosystem vulnerability to systematically examine basin scale topology, critical transition nodes, and the transmission of land system risks under varying disturbance intensities, as well as the associated vulnerability thresholds. However, this study has certain limitations. Transition matrices for 2020–2023 are treated as stationary, and social and economic drivers are exogenous. In addition, although ecosystem service valuation based on equivalent factors contains uncertainty associated with coefficient selection, the primary focus of this study is to evaluate the threshold responses and cascading characteristics of ecological vulnerability under land use change. Previous studies using the equivalent factor method reported relatively low sensitivity coefficients and demonstrated stable valuation results under substantial coefficient variation (Yue *et al* 2007), while further refinement of parameter uncertainty still deserves additional investigation. Moreover, future work should further incorporate these uncertainties, explore dynamic capacity limits, and integrate the cascade model with hydrological and economic modules. Extending the analysis to sequences covering multiple decades and biodiversity outcomes will strengthen causal inference. Despite these limitations, this framework provides a critical foundation for understanding the vulnerability of land systems in China and offers actionable insights for ecosystem management.

Acknowledgment

This study was supported by the National Key Research and Development Program of China (2024YFC3213700), the National Natural Science Foundation of China (52239002 and 32361143871), and the Discipline Innovative Engineering Plan (111 Program, B14002). The data set is provided by Data Center for Resources and Environmental Sciences, Chinese Academy of Sciences (RESDC).

Data availability statement

The data that support the findings of this study are openly available at the following URL/DOI: https://www.resdc.cn/DOI/DOI.aspx?DOIID=54.

Supplementary Methods and Table available at https://doi.org/10.1088/1748-9326/ae83cb/data1.

Author contributions

Xixi Liu 0000-0002-4160-1983
Data curation (equal), Formal analysis (equal), Investigation (equal), Visualization (equal), Writing – original draft (equal)

Zheng Li 0000-0002-3358-9478
Methodology (equal)

Yilin Zhao
Visualization (supporting)

David Makowski 0000-0001-6385-3703
Conceptualization (equal), Methodology (equal)

Xingyu Ren
Investigation (supporting)

Mengyu Zhang
Formal analysis (supporting)

Hong Yang
Methodology (equal)

Wenfeng Liu 0000-0002-8699-3677
Conceptualization (lead), Funding acquisition (lead), Project administration (lead), Supervision (lead), Writing – review & editing (equal)

References

Bao Z J, Cao Y J, Ding L J, Han Z X and Wang G Z 2008 Dynamics of load entropy during cascading failure propagation in scale-free networks *Phys. Lett. A* **372** 5778–82

Bodin Ö *et al* 2019 Improving network approaches to the study of complex social–ecological interdependencies *Nat. Sustain.* **2** 551–9

Cao W, Liu T and Wang X 2022 Effects of soil properties on vegetation community composition across a semiarid ecosystem *J. Arid Environ.* **198** 104700

Cheng H, Wang W, van Oel P R, Lu J, Wang G and Wang H 2021 Impacts of different human activities on hydrological drought in the Huaihe River Basin based on scenario comparison *J. Hydrol.* **37** 100909

Cinner J E and Barnes M L 2019 Social dimensions of resilience in social–ecological systems *One Earth* **1** 51–56

Estrada E and Bodin Ö 2008 Using network centrality measures to manage landscape connectivity *Ecol. Appl.* **18** 1810–25

Felipe-Lucia M R *et al* 2020 Land-use intensity alters networks between biodiversity, ecosystem functions, and services *Proc. Natl Acad. Sci. USA* **117** 28140–9

Felipe-Lucia M R *et al* 2022 Conceptualizing ecosystem services using social–ecological networks *Trends Ecol. Evol.* **37** 211–22

Feng D, Bao W, Fu M, Zhang M and Sun Y 2021 Current and future land use characters of a national central city in eco-fragile region—a case study in Xi'an City based on FLUS model *Land* **10** 286

Fu X, Xu X and Li W 2024 Cascading failure resilience analysis and recovery of automotive manufacturing supply chain networks considering enterprise roles *Physica A* **634** 129478

Hamilton M, Fischer A P and Ager A 2019 A social–ecological network approach for understanding wildfire risk governance *Glob. Environ. Change* **54** 113–23

Han Y, Zhao W and Pereira P 2026 Integrating land degradation states and trends to identify priority areas for ecological restoration in China's drylands *Environ. Impact Assess. Rev.* **118** 108269

He J, Wang Q and Chen T 2025 Changes in network characteristics and risk identification of land ecosystems in the southwest China *Acta Ecol. Sin.* **45** 5363–77 [In Chinese]

He L, Shen J and Zhang Y 2018 Ecological vulnerability assessment for ecological conservation and environmental management *J. Environ. Manage.* **206** 1115–25

Hong W, Jiang R, Yang C, Zhang F, Su M and Liao Q 2016 Establishing an ecological vulnerability assessment indicator system for spatial recognition and management of ecologically vulnerable areas in highly urbanized regions: a case study of Shenzhen, China *Ecol. Indic.* **69** 540–7

Hou L, Xia F, Chen Q, Huang J, He Y, Rose N and Rozelle S 2021 Grassland ecological compensation policy in China improves grassland quality and increases herders' income *Nat. Commun.* **12** 4683

Jarillo J, Cao-garcía F J and De Laender F 2022 Spatial and ecological scaling of stability in spatial community networks *Front. Ecol. Evol.* **10** 861537

Jiang W, Wu T and Fu B 2021 The value of ecosystem services in China: a systematic review for twenty years *Ecosyst. Serv.* **52** 101365

Li Q, Zheng B, Tu B, Yang Y, Wang Z, Jiang W, Yao K and Yang J 2020 Refining urban built-up area via multi-source data fusion for the analysis of dongting lake eco-economic zone spatiotemporal expansion *Remote Sens.* **12** 1797

Lin G C S and Ho S P S 2003 China's land resources and land-use change: insights from the 1996 land survey *Land Use Policy* **20** 87–107

Lu F *et al* 2018 Effects of national ecological restoration projects on carbon sequestration in China from 2001 to 2010 *Proc. Natl Acad. Sci. USA* **115** 4039–44

Luo M, Jia X, Zhao Y, Zhang P and Zhao M 2024 Ecological vulnerability assessment and its driving force based on ecological zoning in the Loess Plateau, China *Ecol. Indic.* **159** 111658

Lv X, Xiao W, Zhao Y, Zhang W, Li S and Sun H 2019 Drivers of spatio-temporal ecological vulnerability in an arid, coal mining region in Western China *Ecol. Indic.* **106** 105475

Malik H A M, Abid F, Wahiddin M R and Bhatti Z 2017 Robustness of dengue complex network under targeted versus random attack *Complexity* **2017** 1–12

Munguia-Vega A, Zepeda-dominguez J A, Perez-alarcon M F, Amador-castro I G, Fulton S, Walther M, Rodriguez-fuentes M, Fumero-andreu C M and Torre J 2022 Social–ecological networks and connectivity within and between two communities of small-scale fishers in Mexico *Ecol. Soc.* **27** 24

National Development and Reform Commission 2024 Compilation of cost and benefit data of national agricultural products—2024

Nguyen K-A and Liou Y-A 2019 Global mapping of eco-environmental vulnerability from human and nature disturbances *Sci. Total Environ.* **664** 995–1004

Nie S and Li H 2023 Analysis of construction networks and structural characteristics of Pearl River Delta and surrounding cities based on multiple connections *Sustainability* **15** 10917

Niu H, Xiu Z and Xiao D 2024 Impact of land-use change on ecological vulnerability in the Yellow River Basin based on a complex network model *Ecol. Indic.* **166** 112212

Novi Inverardi P L and Tagliani A 2023 Probability distributions approximation via fractional moments and maximum entropy: theoretical and computational aspects *Axioms* **13** 28

Pattanayak H S, Verma H K and Sangal A L 2022 Lengthening of average path length in social networks due to the effect of community structure *J. King Saud. Univ.* **34** 8401–21

Peng J, Zhang Z, Lin Y, Tang H, Xu Z and Zheng H 2024 Unveiling decoupled social-ecological networks of Great Lake Basin *Ecosyst. Services Approach* **12** e2024EF004994

Ren L, Wang M, Li C and Zhang W 2002 Impacts of human activity on river runoff in the northern area of China *J. Hydrol.* **261** 204–17

Sala O E *et al* 2000 Global biodiversity scenarios for the year 2100 *Science* **287** 1770–4

Shang Y 2019 Subgraph robustness of complex networks under attacks *IEEE Trans. Syst. Man Cybern. Syst.* **49** 821–32

Sietz D, Niamir A, Müller D, Hickler T, Kanemoto K, Moran D D and Thonicke K 2025 Mapping human-nature archetypes to guide global biodiversity, food security, and land-use policy *One Earth* **8** 101416

Smart A G, Amaral L A N and Ottino J M 2008 Cascading failure and robustness in metabolic networks *Proc. Natl Acad. Sci. USA* **105** 13223–8

Song G, Li Z, Yang Y, Semakula H M and Zhang S 2015 Assessment of ecological vulnerability and decision-making application for prioritizing roadside ecological restoration: a method combining geographic information system, Delphi survey and Monte Carlo simulation *Ecol. Indic.* **52** 57–65

Turner B L *et al* 2003 A framework for vulnerability analysis in sustainability science *Proc. Natl Acad. Sci. USA* **100** 8074–9

Wang J-W and Rong L-L 2009 Cascade-based attack vulnerability on the US power grid *Safe Sci.* **47** 1332–6

Wang Z, Yang Y, Chen G, Wu J and Wu J 2021 Variation of lake-river-aquifer interactions induced by human activity and climatic condition in Poyang Lake Basin, China *J. Hydrol.* **595** 126058

Wei Z, Liang X, Chen H, Yang M, Shi J, Li H and Lui R 2024 Ecosystem vulnerability assessment based on ecosystem services and analysis of its drivers: a case of the Guanzhong region, China *Environ. Dev. Sustain.* **28** 17897–920

Winkler K, Fuchs R, Rounsevell M and Herold M 2021 Global land use changes are four times greater than previously estimated *Nat. Commun.* **12** 2501

Wu Y, Huang L, Zhao C, Chen M and Ouyang W 2021 Integrating hydrological, landscape ecological, and economic assessment during hydropower exploitation in the upper Yangtze River *Sci. Total Environ.* **767** 145496

Xie G D, Lu C X, Leng Y F, Zheng D and Li S C 2003 Ecological assets valuation of the Tibetan Plateau *J. Nat. Resour.* **18** 189–96

Xie G D, Zhang C X, Zhang L M, Chen W H and Li S M 2015 Improvement of the evaluation method for ecosystem service value based on per unit area *J. Nat. Resour.* **30** 1243–54

Xie G, Zhang C, Zhen L and Zhang L 2017 Dynamic changes in the value of China's ecosystem services *Ecosyst. Serv.* **26** 146–54

Xiong C, Ren H, Xu D and Gao Y 2024 Spatial scale effects on the value of ecosystem services in China's terrestrial area *J. Environ. Manage.* **366** 121745

Xu X, Liu J, Zhang S, Li R, Yan C and Wu S State Key Laboratory of Resources and Environmental Information System, Institute of Geographic Sciences and Natural Resources Research, Chinese Academy of Sciences, Beijing, China 2026 China Multi-Period Land Use/Land Cover Remote Sensing Monitoring Dataset (CNLUCC) *Data Center for Resources and Environmental Sciences, Chinese Academy of Sciences (RESDC)* (https://doi.org/10.12078/2018070201) (available at: https://www.resdc.cn/DOI/DOI.aspx?DOIID=54)

Xu X, Lu C, Shi X and Ding Y 2010 Large-scale topography of China: a factor for the seasonal progression of the Meiyu rainband? *J. Geophys. Res. Atmos.* **115** D02110

Yang L, Niu T, Yu Q, Zhang X and Wu H 2022 Relationship between topological structure and ecosystem services of forest grass ecospatial network in China *Remote Sens.* **14** 4700

Yang Z, Cai Y and Mitsch W J 2015 Ecological and hydrological responses to changing environmental conditions in China's river basins *Ecol. Eng.* **76** 1–6

Yin S, Yi Y, Liu Q, Luo Q and Chen K 2022 A review on effects of human activities on aquatic organisms in the Yangtze River Basin since the 1950s *River* **1** 104–19

Yu G, Liu T, Wang Q, Li T, Li X, Song G and Feng Y 2022 Impact of land use/land cover change on ecological quality during urbanization in the lower yellow River Basin: a case study of Jinan City *Remote Sens.* **14** 6273

Yue S, Zhang S and Yan Y 2007 Impacts of land use change on ecosystem service value in the Northeast China transect *Acta Geograph. Sin.* **62** 879–86 [In Chinese]

Zhang H, Fiszman M, Shin D, Miller C M, Rosemblat G and Rindflesch T C 2011 Degree centrality for semantic abstraction summarization of therapeutic studies *J. Biomed. Inform.* **44** 830–8

Zhang Q, Miao C, Guo X, Gou J and Su T 2023 Human activities impact the propagation from meteorological to hydrological drought in the Yellow River Basin, China *J. Hydrol.* **623** 129752

Zhao J, Li D, Sanhedrai H, Cohen R and Havlin S 2016 Spatio-temporal propagation of cascading overload failures in spatially embedded networks *Nat. Commun.* **7** 10094

Zhao L, Park K, Lai Y-C and Ye N 2005 Tolerance of scale-free networks against attack-induced cascades *Phys. Rev. E* **72** 025104

Zhu N, Ai J, Zeng Z and Zhou C 2023 Exploring the spatial relationship between the ecological topological network and carbon sequestration capacity of coastal urban ecosystems: a case study of Yancheng City, China *Remote Sens.* **15** 4007

Zou T, Chang Y, Chen P and Liu J 2021 Spatial-temporal variations of ecological vulnerability in Jilin Province (China), 2000–2018 *Ecol. Indic.* **133** 108429

Zou T and Yoshino K 2017 Environmental vulnerability evaluation using a spatial principal components approach in the Daxing'anling region, China *Ecol. Indic.* **78** 405–15